ELSEVIER

Materials Chemistry and Physics 65 (2000) 51–56

MATERIALS CHEMISTRY AND PHYSICS

www.elsevier.com/locate/matchemphys

Photoluminescence and electron paramagnetic resonance studies of defect centers in porous silicon

Hang-Ting Lue[a], Bang-Yuh Huang[b], Juh-Tzeng Lue[b,*]

[a] *Department of Electronic Engineering, National Chao Tung University, Hsin Chu, Taiwan*

[b] *Department of Physics, National Tsing Hua University, Hsin Chu, Taiwan*

Received 25 June 1999; received in revised form 26 November 1999; accepted 30 November 1999

Abstract

Photoluminescence (PL) and electron spin resonance (ESR) spectrometers were exploited to study the P_b defect centers in porous silicon (PS) under various heat treatments. The breaking of Si–H_x and Si–O–H bonds in PS by thermal annealing changes the emission wavelength and increases the recombination centers resulting in degrading the PL intensity. Four kinds of dangling bonds on interfaces of silicon (1 1 1), (1,−1,−1), (−1,1,−1), and (−1,−1,1) faces and SiO_2 with C_{3V} symmetry were identified. The skeleton structure of PS collapsed under thermal annealing. Annealing in hydrogen gas, which is controvertible to the pervasive anticipation, cannot passivate the dangling bonds introduced at high temperatures.

Keywords: Photoluminescence; Electron paramagnetic resonance; Porous silicon

1. Introduction

Silicon material, although, has well-developed technology and widely utilized in electronic devices, the intrinsic indirect-gap behavior limits its use in photonic devices. The discovery of strong photoluminescence [1–3] of porous silicon (PS) was prospected to have pragmatic uses in light emitting devices for the integration of modulating light sources, photo-detectors and amplifiers from the implementation of a simple silicon material. In our previous works, we have demonstrated [4] that quantum size effect is not crucial to generate photo-luminescence (PL) in PS. Comparing the PS with siloxane ($Si_6O_3H_6$) like materials [5], we neither observed [6], the infrared (IR) absorption peak of Si–O–H vibration bond nor its Raman peak at 514 cm^{-1} for the freshly prepared PS samples. Only samples stored in air for several days, the PL of the above lines show up with the intensity of other lines being much larger than that of the freshly prepared sample adducing that the IR absorption peaks of Si–H_x, or Si–O–H bonds are found on the oxidized sample. The PL intensity also diminishes with the decrease of Si–H_x bond density due to vacuum annealing informing that the breaking of Si–H_x bonds implies the formation of non-radiate recombination centers to degrade the PL intensity. Accordingly, the defects in PS play an essential role of the PL.

In spite of the existence of several reports [7–10] on electron spin resonance (ESR) studies of PS, many itinerant features of PS defects are not revealed, and heat treatment effects on the ESR are not fully studied. In this work, we attempt to study the point defects in PS by electron spin resonance spectrometry. This technique allows us to address the site of a particular defect, the structure symmetry, and the spin density change due to annealing effect.

2. Mechanisms of photoluminescence

The origins of photoluminescence in general arise from the radiative decay of atoms or molecules from the excited energy levels such as in organic dyes and polymers. In direct energy gap semiconductors, the recombination of electrons and holes from the conduction and valence bands, respectively, evoke the luminescence. For silicon, an indirect energy gap material, the PL is extremely small and can be observed only at very low temperatures. Discrete energy levels split from the continuous conduction band [11,12] showing a direct transition arise due to the quantum confinement of nano-particles. The strong PL as observed even at room temperature of PS suggesting an indirect to direct band gap transition. Unfortunately further investiga-

* Corresponding author.

0254-0584/00/$ – see front matter
PII: S0254-0584(00)00213-3

tions found that almost identical PL and Raman spectra of artificially synthesized silioxane and PS, and the lost of PL for pure silicon nano-particles as small as 4 nm alluding that quantum size effect is not crucial to the PL in PS [4]. In this work, we attempt to study the interplay between the changes of chemical adsorption molecules and defects in PS affecting the PL spectra by thermal annealing, and expect to yield a real consensus on this fact.

3. Defect centers in porous silicon

Native defects generated during crystal growth such as vacancies, antisites and interstitial control the photonic properties for intrinsic semiconductors. Among the possible intrinsic defects, the isolated silicon dangling bonds demonstrate themselves to be the dominant interface defects, which crucially control the photo-luminescence efficiency.

The point defects in PS, can be a P_{bo}-like (i.e. Si≡Si), a P_{b1} (i.e. Si≡SiO_2), and a P_b-like center. The ESR of P_{bo} yields a broad and small signal-to-noise ratio signal, while the P_{b1} is essentially capricious with thin oxides [8]. The most intricate P_b defects are associated with silicon dangling bonds and can be classified to three types. They are positive charged D^+, the negative charged D^-, and the neutral D°. The D° has unpaired electrons with a net spin moment and can be readily detected by an ESR spectrometer. The rapture of one of the tetrahedral sp^3 valence electrons leaves one unoccupied dangling bond. The annealing of PS in hydrogen gas can passivate the dangling bonds by hopping process [13]. On the other hand, heating the sample in vacuum or in air, the hydrogen atoms may escape from the weak Si–H bonds and restore to the dangling states. Porous silicon, which is modified from crystalline silicon, has a lower symmetry of C_{3v} than its original diamond T_d structure. The porous structure implies a large surface area to be oxidized when stored in air, which invokes dangling bonds at the interface between silicon and SiO_2.

The commonly specified P_b centers [3,14,15] are the point defects concealed at the interface of Si(1 1 1)/SiO_2 as shown in Fig. 2. There are four paramagnetic centers belonging to the P_b defects named as S_1=(1 1 1), S_2=(1,−1,−1), S_3=(−1,1,−1) and S_4=(−1,−1,1) corresponding to the dangling bonds at the interface of the specified Si surfaces and oxides.

4. The *g*-tensors in ESR studies

For a defect center with a free spin $\vec{S}$, the spin Hamiltonian in a magnetic field $\vec{H}$ is [16–18]

$$\Re = \beta \vec{S} \overline{\overline{g}} \cdot \vec{H}, \tag{1}$$

where β is the electron Bohr magneton, $\vec{g}$ is a dyadic tensor. Taking a Cartesian coordinates (*xyz*), the magnetic field H has components of

$$\vec{H} = H(\ell_x \hat{x} + \ell_y \hat{y} + \ell_z \hat{z}), \tag{2}$$

where, ℓ_x, ℓ_y and ℓ_z are the cosines along the $\hat{x}$, $\hat{y}$, and $\hat{z}$ axes, respectively. The spin Hamiltonian Eq. (1) then can be written as

$$\Re = \beta \cdot H(\ell_x, \ell_y, \ell_z) \begin{pmatrix} g_{xx} & g_{xy} & g_{xz} \\ g_{yx} & g_{xy} & g_{yz} \\ g_{zx} & g_{zy} & g_{zz} \end{pmatrix} \begin{pmatrix} s_x \\ s_y \\ s_z \end{pmatrix}, \tag{3}$$

where (s_x, s_y, s_z) are the components of the spin along the Cartesian coordinates. We can define an effective g_{eff} such as

$$\begin{aligned} g_{\text{eff}}^2 &= (\ell_x, \ell_y, \ell_z)(\overline{\overline{g}}^{\sim} \cdot \overline{\overline{g}}^{\sim}) \begin{pmatrix} \ell_x \\ \ell_y \\ \ell_z \end{pmatrix} \\ &= (\ell_x, \ell_y, \ell_z) \begin{pmatrix} (g^2)_{xx} & (g^2)_{xy} & (g^2)_{xz} \\ (g^2)_{yx} & (g^2)_{yy} & (g^2)_{yz} \\ (g^2)_{zx} & (g^2)_{zy} & (g^2)_{zz} \end{pmatrix} \begin{pmatrix} \ell_x \\ \ell_y \\ \ell_z \end{pmatrix} \end{aligned} \tag{4}$$

where $\overline{\overline{g}}^{\sim}$ is the transpose conjugate $\overline{\overline{g}}$.

In this case, the Zeeman splitting energy ΔE for a spin 1/2 transition can be readily written as $\Delta E = \beta g_{\text{eff}} H$ with

$$\begin{aligned} (\Delta E)^2 &= \beta^2 g_{\text{eff}}^2 H^2 = \beta^2 (\vec{H} \cdot \overline{\overline{g}}^{\sim}) \cdot (\overline{\overline{g}} \cdot \vec{H}) \\ &= \beta^2 \vec{H} \cdot g^2 \cdot \vec{H} \end{aligned} \tag{5}$$

The elements $(g^2)_{ij}$ can be determined from the ESR rotating spectra as addressed below. If the *y*-axis of the sample surface (the *xy* plane) is rotated with respect to the magnetic field $\hat{H}$ with an intersection angle θ, then

$$g_{\text{eff}}^2 = (g^2)_{xx} \sin^2\theta + 2(g^2)_{xy} \sin\theta \cos\theta + (g^2)_{yy} \cos\theta \tag{6}$$

We can readily determine $(g^2)_{yy}$ at θ=0°, $(g^2)_{xx}$ at θ=90°, and $(g^2)_{xy}$ at θ=45°, respectively. In the same way, with different rotating plane, we can evaluate the six tensor elements $(g^2)_{ij}$=$(g^2)_{ji}$ by which the g^2 is diagonalized to yield the principle values such as

$$g^2 = \begin{pmatrix} g_x^2 & 0 & 0 \\ 0 & g_y^2 & 0 \\ 0 & 0 & g_z^2 \end{pmatrix} \tag{7}$$

For crystals have axial symmetry such as hexagonal, tetragonal, and trigonal, then

$$g = \begin{pmatrix} g_\perp & 0 & 0 \\ 0 & g_\perp & 0 \\ 0 & 0 & g_\parallel \end{pmatrix} \tag{8}$$

where $g_\parallel$ and $g_\perp$ are the *g*-values obtained for the magnetic field H to be parallel or perpendicular to the symmetry axis. In this case, the experimental resonant position occurs at

$$H = \frac{h\nu}{g\beta}, \quad \text{with} \quad g = (g^2 \cos^2\theta + g_\perp^2 \sin^2\theta)^{1/2} \tag{9}$$

where θ is the angle between the dangling bond $\vec{S}_{ii}$ and the magnetic field $\vec{H}$. In this experiment, we rotate the PS

surfaces with respect to the c-axis by several angles δ to detect the spectra.

The transform matrix $\overline{\overline{R}}$ that rotates the spin $\vec{S}_i$ by an angle δ to yield

$$\theta = \cos^{-1} \vec{H} \cdot \overline{\overline{R}} \cdot \vec{S}_i \tag{10}$$

can be derived as follows. Firstly, we decompose the spin vector $\vec{S}_i$ into components of $\vec{S}_{i\ell}$ and $\vec{S}_{it}$ to be parallel and perpendicular to the c-axis, respectively. From $\vec{S}_{it}$, we then take a third vector $\vec{S}'_{it}$ to be perpendicular both to $\vec{S}_{it}$ and $\hat{c}$, such as

$$\vec{S}'_{it} = \hat{c} \times \vec{S}_{it} = \hat{c} \times (\vec{S}_i - (\vec{S}_i \cdot \hat{c})) \text{ and } \left|\vec{S}'_{it}\right| = \left|\vec{S}_{it}\right|. \tag{11}$$

On rotating $\vec{S}_i$ with respect to the c-axis by an angle δ, the $\vec{S}_{i\ell}$ retains its original value while $\vec{S}_{it}$ moves to a new value

$$\vec{S}_{it}(\delta) = \vec{S}_{it} \cos\delta + \vec{S}'_{it} \sin\delta. \tag{12}$$

The new spin direction $\vec{S}_i(\delta)$ becomes

$$\begin{aligned}\vec{S}_i(\delta) = \vec{S}_{i\ell} + \vec{S}_{it}(\delta) = (\vec{S}_i \cdot \hat{c})\hat{c} + (\vec{S}_i - (\vec{S}_i \cdot \hat{c})\hat{c})\cos\delta \\ +(\vec{S}_i - (\vec{S}_i \cdot \hat{c}))\sin\delta = \overline{\overline{R}} \cdot \vec{S}_i\end{aligned} \tag{13}$$

The transform matrix is explicitly written as

$$R(\delta) = \begin{pmatrix} c_x^2(1-\cos\delta)+\cos\delta & c_x c_y(1-\cos\delta) - c_z\sin\delta & c_x c_z(1-\cos\delta)+c_y\sin\delta \\ c_x c_y(1-\cos\delta)+c_z\sin\delta & c_y^2(1-\cos\delta)+\cos\delta & c_y c_z(1-\cos\delta)-c_x\sin\delta \\ c_x c_z(1-\cos\delta)-c_y\sin\delta & c_y c_z(1-\cos\delta)+c_x\sin\delta & c_z^2(1-\cos\delta)+\cos\delta \end{pmatrix} \tag{14}$$

where c_x, c_y, c_z are the direction cosines of $\hat{c}$-axis. After a tedious manipulation of Eqs. (10)–(13), we obtain the effective g values in terms of the rotating angle δ for the defect centers S_1, S_2, S_3, S_4. With the magnetic field $\vec{H}$ to be along $\langle 1,0,0\rangle$, we can derive

$$\begin{aligned} g_{\text{eff}}\{S_1\} = \frac{1}{\sqrt{6}}\Big[3(g_\parallel^2+g_\perp^2)+(-g_\parallel^2+g_\perp^2)\cos(2\delta) \\ -2\sqrt{2}\left(g_\parallel^2-g_\perp^2\right)\sin(2\delta)\Big]^{1/2} \end{aligned}$$

$$\begin{aligned} g_{\text{eff}}\{S_2\} = \frac{1}{\sqrt{6}}\Big[3\left(g_\parallel^2+g_\perp^2\right)+\left(-g_\parallel^2+g_\perp^2\right)\cos(2\delta) \\ +2\sqrt{2}\left(g_\parallel^2-g_\perp^2\right)\sin(2\delta)\Big]^{1/2} \end{aligned}$$

$$\begin{aligned} g_{\text{eff}}\{S_3\} &= \frac{1}{\sqrt{6}}\Big[g_\parallel^2+5g_\perp^2+(g_\parallel^2-g_\perp^2)\cos(2\delta)\Big]^{1/2} \\ &= g_{\text{eff}}\{S_4\} \end{aligned} \tag{15}$$

The measured g-values at various rotation angles can be deconvoluted to yield the principle g-values.

5. Electron spin resonance measurement

The p-type (1 0 0) and (1 1 1) silicon wafers with resistivity of 0.01–0.02 Ω cm were vacuum evaporated with aluminum on the backside and rapidly thermally annealed (RTA) at 500°C for 10 min to form an ohmic contact. The anodization method followed the same procedures as previously reported [6]. The heavily doped PS film can be easily detached from its original Si substrate by sharply increasing the current to 500 ma for 30 s at the final anodization process. The fragile thin PS was then tailored in a proper size of $3\times10\times0.1\,\text{mm}^3$ and loaded in a TE_{104} dual microwave cavity. A Brucker EMX-10 ESR spectrometer operating at x-band was exploited for this detection. The data were assessed at every 5° rotating angles from 0 to 180°. The experimental data for rotating the crystal face (0,−1,1) with respect to the magnetic field $\hat{H}$ at various angles are plotted in Fig. 1.

The experimental data are simulated to yield the true resonance positions for the four P_b point defects by least-mean-square curve fitting. Rotating the crystal axis $\langle 0,-1,1\rangle$, the C_{3v} symmetry conveys that the defect centers at S_3=(−1,1,−1) and S_4=(−1,−1,1) do have the same angular dependence on the ESR spectra.

Three resonance centers S_1, S_2 and S_3=S_4 have ESR intensity ratio of 1:1:2. Assuming a homogenous broadening, the ESR line-shape can be accessed by taking the composition of three Lorentzian lines at various field x such as

$$Y(x) = -\sum_{i=t}^{3} \frac{8I_i(-\lambda_i + x)}{\Gamma_i\left[1+(4(-\lambda_i+x)^2)/\Gamma_i\right]^2} \tag{16}$$

where λ_i are the resonance magnetic fields and Γ_i are the full-width at half-maximum (FWHM) of each spectrum.

The least-mean-square fitting [19] is exploited to simulate the experimental data and extract the resonance field λ_i. The smooth curves adjoined with the experimental data points as plotted in Fig. 1 yield the resonant g-values at each rotation angles for the four P_b centers. Fig. 2 portraits the variation of g-value with rotation angles δ with respect to the four P_b defect centers. The four P_b defects in ideal should have the same principle g-value, but on account of the slight deviation of bond angles for dangling bonds on different faces, they imply three g-values as depicted in Table 1. The average g-values are given by $g_\parallel$=2.0016±0.0003, $g_\perp$=2.0089±0.0003 for P_b centers along the $\langle 1\,1\,1\rangle$ axis. The angular dependence of g-values of the P_b centers turns out that the virgin PS belongs to the C_{3v} symmetry.

6. Photoluminescence measurement

The PL spectra of PS crucially depend on the surface absorbed molecules such as Si–H_x, Si–O–H, and Si–O–Si

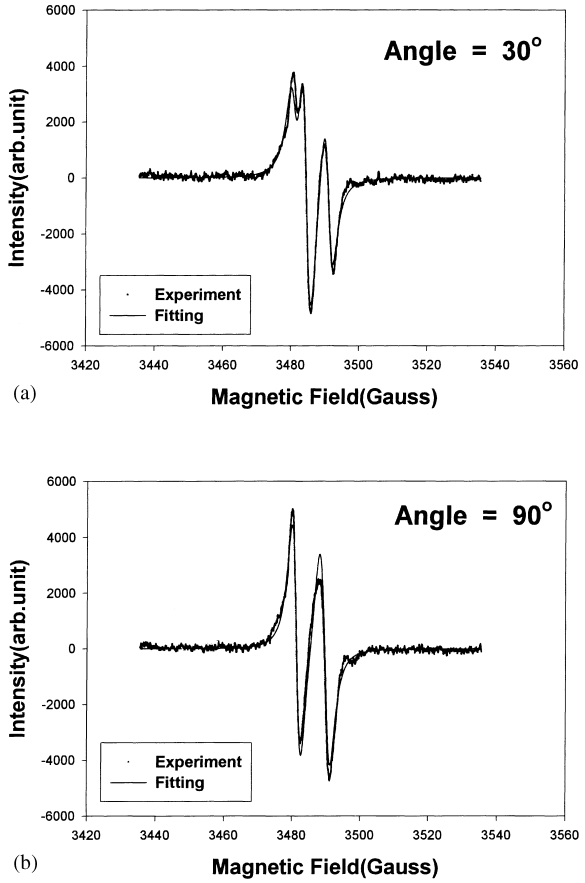

Fig. 1. Typical ESR spectra at various angles δ for the rotating axis along $\langle 0,-1,1\rangle$ and the magnetic field $\hat{H}$ along $\langle 1\,0\,0\rangle$ at angles of 30° and 90°.

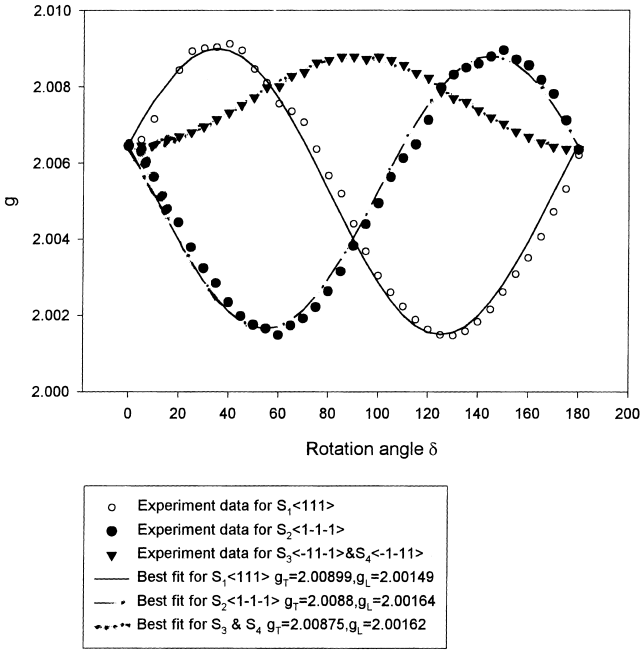

Fig. 2. The g-values at various rotating angles δ for the theoretical calculation by exploiting Eq. (11) (the smooth curves), and the experimental data fitting for the ●, S_1, O, S_2, ∇, S_3=S_4 of P_b centers.

Table 1
The principle g-values for different P_b defect centers

P_b defects	$g_\parallel$	$g_\perp$
S_1	2.0015±0.0003	2.0089±0.0003
S_2	2.0016±0.0003	2.0088±0.0003
S_3=S_4	2.0016±0.0003	2.0087±0.0003

while the immersing environment determines the surface chemical bonds and the crystalline size determining the interaction field strength between radicals which yield the shift of the PL peak. In order to immunize from its direct contact with air, we embedded the PS powder detached from the Si wafers into the silica glass by sol–gel method [20,21] and then analyzed the changes of PL with heat treatment.

The complex solution composed of 20 ml of tetra-ethyl-ortho-silicate ($Si(OC_2H_5)_4$) with 20 ml of ethanol, 16 ml of de-ionized water and the PS powder were mixed uniformly by a magnetic stirrer for 4 h. The mixed solution was poured into a plastic disc with a cover cape and waited to gel for 2 days. The gel was dried in air at room temperature for 1 week. The PL was measured at various temperatures by mounting the sample on a heating head. For temperatures below 120°C, the spectra as shown in Fig. 3 saliently increases from room temperature to 62°C and then gradually decreases until 162°C. Above which the PL peak shifts rigorously from its original 700 to 530 nm, and the intensity increases with temperatures again. An adducing from the vanishing of some of the Fourier transform infra-red (FTIR) spectral lines after annealing, we may tacitly assume that the peak near 700 nm is attributed from the Si–H_x, and 600 nm from the Si–O–H attached on the PS walls. At temperatures below 162°C, the transformation of SiH_x and Si–O–H is reversible. For temperatures further increasing above 270°C, the PL peak shifts to 530 nm and the intensity decreases with

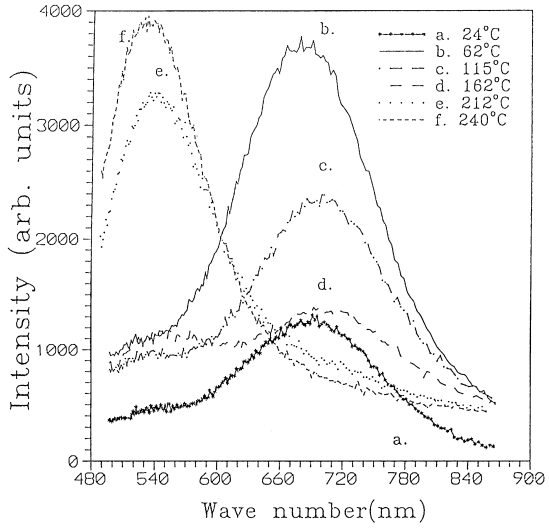

Fig. 3. The PL of PS powder embedded in silica glass measured at various temperatures. The spectra measured between 24 and 162°C are reversible.

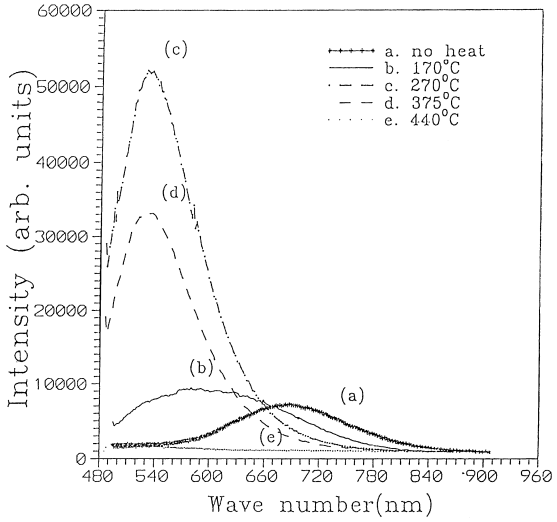

Fig. 4. The PL of PS powder embedded in silica glass measured from 24 to 440°C.

temperatures again as shown in Fig. 4. This evidence might be due to the decomposition of Si–H_x and Si–OH bonds to form Si–O–Si bonds and yielding the 530 nm line. This decomposition is irreversible. As temperature increases, the recombination centers so called dangling bonds are formed by the decomposition of the adsorbed chemical radicals resulting in the decrease of PL intensity. For temperatures above 440 C, the PL vanishes.

7. Discussion

In this work, the ESR spectra are exploited to study the change of the density of defect centers by thermal annealing. The ESR line-shapes almost unchanged at low temperatures, while after 500°C thermal annealing in vacuum, the signals survive in three resonance lines with intensity ratio changing to nearly 1:1:1 and cannot be simulated by the C_{3v} symmetry. Possibly due to the collapse of skeleton structure of PS, a newly created defect center which is almost isotropic with the rotation angle δ can be detected. We have plotted the ESR spectra for the virgin and the annealed sample on the same chart to compare their shifts in resonance position as shown in Fig. 5. The spin density of PS can be readily calculated by comparing the spectral area with that of the referenced DPPH signal, which was simultaneously detected with a dual cavity. The thermal annealing also increases the dangling bonds by breaking the covalent bonds. The higher the temperature, the more the defect centers were created as shown in the isochronal annealing curves of Fig. 6. The Fourier transform infrared (FTIR) spectra as shown in Fig. 7 also reveals the presence of dangling bonds arising from the Si–OH, Si–O–R and Si–O_2 bonds after annealing in air. The oxygen defects are smeared out after 400°C annealing in H_2 but without convincing evidence for vacuum annealed

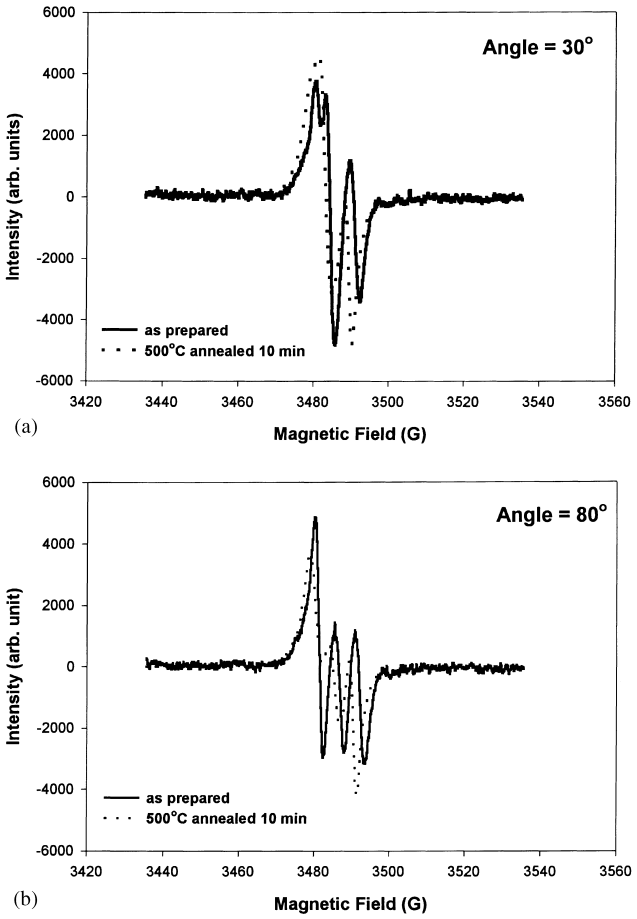

Fig. 5. The ESR spectra for virgin (------), and 500°C annealed for 10 min (. . . . .) PS at rotating angles of (a) 30°and (b) 90°, respectively.

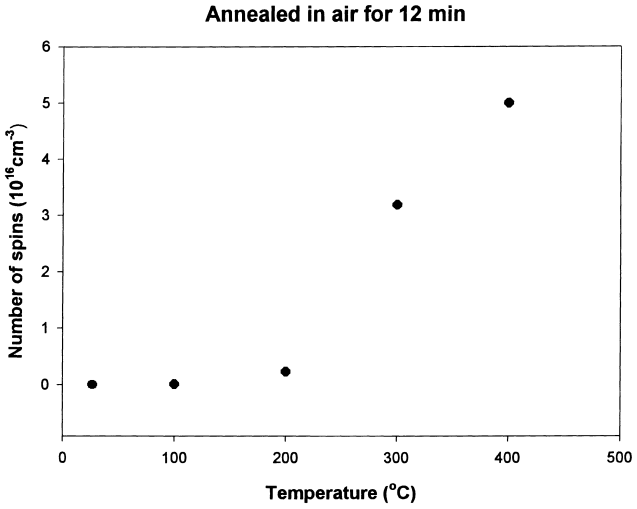

Fig. 6. The change of spin densities for isochronal annealing of PS at various temperatures

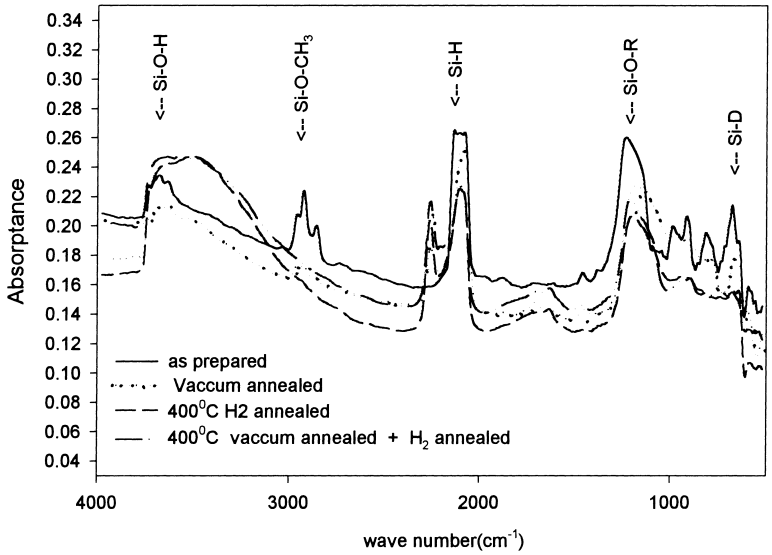

Fig. 7. The FTIR spectra at different annealing conditions.

samples. The degradation of the PL intensity almost follows the increase of defect centers as measured by the ESR spectrometer.

In conclusion, we have studied the point defects of PS arising from the dangling bonds by ESR. The four P_b defects are identified to be $S_1 \cdots S_4$ with C_{3v} symmetry. Thermal annealing at 200–300°C increases the spin density vastly informing that most of the weak bonds of PS have a strength of ∼49 meV which will be broken into dangling bonds above this temperature. Annealing in H_2 gas can passivate the dangling bonds but not for bond broken at high temperatures. The dangling bonds play an essential role of recombination centers and degrade the photoluminescence intensity.

This work was supported by the National Science Council of the Republic of China under contract NSC 88-2112-M007-019.

References

[1] A. Uhlir, Bell System, Technical J. 35 (1956) 333.
[2] D.R. Turner, J. Electrochem. Soc. 105 (1958) 402.
[3] L.T. Canham, Appl. Phys. Lett. 57 (1990) 1046.
[4] S.K. Ma, J.T. Lue, Thin Solid Films 304 (1997) 353.
[5] H.D. Fuch, M. Statzman, M.S. Brandt, Phys. Rev. B. 48 (1993) 2172.
[6] G.S. Chang, J.T. Lue, Thin Solid Films 259 (1994) 275.
[7] H.J. von Bardeleben, D. Stievenard, A. Grosman, C. Ortega, J. Siejka, Phys. Rev. B 47 (1993) 10899.
[8] Y. Uchida, N. Koshida, H. Kayama, Y. Yamamoto, Appl. Phys. Lett. 63 (1993) 961.
[9] F.C. Rong, J.F. Harvey, E.H. Poindexter, G.J. Gerardi, Appl. Phys. Lett. 63 (1993) 920.
[10] V.Ya. Bratus, S.S. Ishchenko, S.M. Okulov, I.P. Vorona, H.J. von Bardeleben, Schoisswohl, Phys. Rev. B 50 (1994) 15449.
[11] W.C. Huang, J.T. Lue, Phys. Rev. B 49 (1994) 17297.
[12] W.C. Huang, J.T. Lue, J. Phys. Chem. Solids 58 (1997) 1529.
[13] P.J. Caplan, E.H. Poindexter, B.E. Deal, R.R. Razonk, J. Appl. Phys. 52 (1981) 879.
[14] A. Stesmans, Appl. Phys. Lett. 48 (1986) 972.
[15] A. Stesmans, Phys. Rev. B 45 (1992) 9051.
[16] E.H. Poindester, P.J. Caplan, B.E. Deal, R.R. Razonk, J. Appl. Phys. 52 (1981) 879.
[17] J.T. Lue, Nuovo cimento IL, 31B (1976) 372
[18] J.E. Wertz, J.R. Bolton, Electron Spin Resonance, McGraw-Hill, New York, 1986.
[19] C.F. Gerald, Applied Numerical Analysis, Addison-Wesley, 1983, p. 465.
[20] J.T. Lue, W.C. Huang, S.K. Ma, Phys. Rev. B 51 (1995) 14570.
[21] S.K. Ma, J.T. Lue, Solid State Commun. 97 (1996) 979.